Nano Research
DOI 10.1007/s12274-014-0665-y
Research Article
ISSN 1998-0124
CN 11-5974/O4

Crystal-oriented wrinkles with origami-type junctions in few-layer h-BN

Camilla K. Oliveira[1†], Egleidson F. A. Gomes[1], Mariana C. Prado[1], Thonimar V. Alencar[1], Regiane Nascimento[1], Leandro M. Malard[1], Ronaldo J. C. Batista[2], Alan B. de Oliveira[2], Helio Chacham[1], Ana M. de Paula[1] and Bernardo R. A. Neves[1*]

Nano Res., **Just Accepted Manuscript** • DOI: 10.1007/s12274-014-0665-y
http://www.thenanoresearch.com on December 1 2014

Just Accepted

TSINGHUA UNIVERSITY PRESS Springer

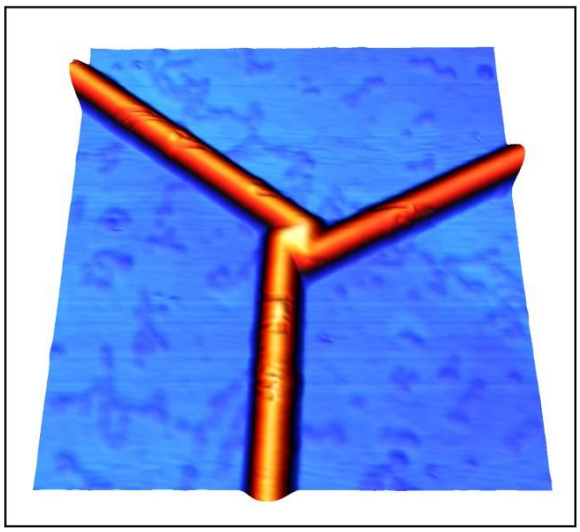

The morphology and optical response of heat-treated hexagonal boron nitride few-layer flakes reveal the formation of linear wrinkles along well-defined crystallographic directions. They form a network of origami-type junctions throughout the sample accommodating layer strain. The results indicate that this process may be a general property of several 2D materials under the proper stress-strain conditions with direct consequences on device strain engineering.

Crystal-oriented wrinkles with origami-type junctions in few-layer h-BN

Camilla K. Oliveira[1†], Egleidson F. A. Gomes[1], Mariana C. Prado[1], Thonimar V. Alencar[1], Regiane Nascimento[1], Leandro M. Malard[1], Ronaldo J. C. Batista[2], Alan B. de Oliveira[2], Helio Chacham[1], Ana M. de Paula[1] and Bernardo R. A. Neves[1*]

[1] Departamento de Física, ICEx, Universidade Federal de Minas Gerais – UFMG, C.P. 702, 30123-970 – Belo Horizonte – Brazil.

[2] Departamento de Física, ICEB, Universidade Federal de Ouro Preto – UFOP, 35400-000 – Ouro Preto – Brazil

[†] Present address: Departamento de Física, Universidade Federal do Paraná – UFPR, Caixa Postal 19044, 81531-990 – Curitiba – Brazil.

*E-mail: bernardo@fisica.ufmg.br

Abstract

Understanding the layer interplay is key to explore new layered heterostructures formed by the stacking of different 2D materials for device applications. Boron nitride has been shown to be an ideal substrate on which to build graphene devices with improved mobilities. Here we present studies of the morphology and optical response of annealed hexagonal boron nitride few-layer flakes deposited on silicon substrate that reveals the formation of linear wrinkles along well-defined crystallographic directions. They form a network of threefold (mostly) and fourfold (rarely) origami-type junctions throughout the sample and all threefold junctions and wrinkles are formed along the armchair crystallographic direction. Furthermore, molecular dynamics simulations yield, through spontaneous symmetry breaking, wrinkle junction morphologies that are consistent with both the experiments and the proposed origami-folding model. Our findings indicate that this may be a general property of several 2D materials under the proper stress-strain conditions with direct consequences on device strain engineering.

Keywords: Hexagonal boron nitride, 2D materials, wrinkles, origami folding, annealing

1. Introduction

On the macroscale, most materials, regardless of their dimensionality (1D, 2D or 3D), present a conventional stress-strain behavior: they shrink upon compression (compressive stress) and expand under extension (tensile stress) [1]. These materials, when in 2D or 3D structures and under one-dimensional stress, normally expand (shrink) in the direction of a tensile (compressive) stress, while shrinking (expanding) on a perpendicular direction [1]. Auxetic (or negative Poisson's ratio) materials represent a deviation from such standard behavior, as they may simultaneously expand in both parallel and perpendicular directions under a one-dimensional tensile stress [2]. As the length scale gets smaller, towards micro- and nanoscales, additional non-standard stress-strain behavior may appear, such as the negative compressibility (both static [3] and dynamic [4]), including a giant negative compressibility which arises from a giant positive compressibility [5].

Narrowing the focus to 2D systems, these materials present a wealthy variety of physical and chemical properties, leading to a myriad of studies of their properties [6-14]. Due to their layered nature, the formation of wrinkles upon compressive stress could, at first sight, be regarded as an ordinary strain configuration [6-10]. However, both strain and strain gradients are known to alter fundamental physical properties of 2D materials, such as the "pseudomagnetic" quantum Hall effect in graphene [15], the strain photonics in MoS_2 [16] and flexoelectricity in h-BN [17]. As a consequence, even a new term, *straintronics*, has been coined and it is a promising field [6-10, 14, 18]. For this reason, the formation of wrinkles in 2D materials is actually far from ordinary and wrinkle engineering, a direct consequence of strain engineering, may represent a major topic in their investigation. For graphene, the most investigated 2D material, wrinkle formation, characterization and application is already a

subject of intense activity [6-10, 14]. The recently proposed massive fabrication of graphene nanoribbons is just an example [19]. Therefore, in this work, a new non-conventional stress-strain behavior in a 2D material revealed: the formation of crystallographically-oriented origami-type wrinkles in annealed h-BN layers. Using atomic force microscopy (AFM), self-assembly procedures and second-harmonic generation (SHG) experiments, both the morphology and orientation of such wrinkles are studied. A simple phenomenological model and molecular dynamics simulations account for the wrinkle formation mechanism, which indicates it could be a general property of several 2D materials under the proper stress-strain (or wrinkle engineering) conditions.

2. Results

2.1. AFM characterization of annealed h-BN

Figure 1 summarizes the morphological AFM characterization of annealed h-BN flakes and shows topographic images of a few-layer h-BN flake in three different magnifications. The small squares in figure 1a and 1b indicate the regions where figure 1b and 1c were acquired, respectively. It is clearly seen in figure 1 that the annealing treatment produced a well-defined geometric pattern of wrinkles.

Also, the wrinkle orientation is not random, but only occurs at certain angles. As evidenced by their respective Fast-Fourier Transform (FFT) images (insets of figure 1a and 1b), there are mainly three orientations for the wrinkles in figure 1. A quick inspection of this figure reveals that the vast majority of wrinkle junctions is threefold and figure 1b and 1c

show more detailed images of such representative junction. Each wrinkle in figure 1c is around ten nanometers high, as indicated by the color scale, but, in general, wrinkle height in all investigated samples varied from a single nanometer to several tens of nanometers. An interesting feature of figure 1c is the morphology of a typical junction: the wrinkles always connect to each other through the vertexes of a small rotated triangle (in reddish shade in the image center).

2.2. Phosphonic acid decoration

An immediate question which arises from the results in figure 1 is whether there is any registry between the wrinkle orientation and the h-BN lattice. In other words, are the wrinkles crystallographically oriented? Two independent experimental procedures were employed to answer this question: decoration of h-BN with self-assembled octadecylphosphonic acid (OPA) molecules and polarization dependent SHG experiments. Recently, Prado *et. al.* have demonstrated that decoration of graphene with OPA self-assembled monolayers enabled the identification of its crystallographic orientation [20]. OPA is a 2.5 nm-long molecule with a phosphonic acid headgroup attached to a long linear alkyl chain and it self-assembles on graphene with its axis parallel to the surface, in a configuration that allows the headgroup of adjacent molecules to interact via hydrogen bonding, forming rippled domains detected by AFM [20]. *Ab initio* calculations and AFM images showed that these ripples are oriented along the graphene armchair direction [20]. Since h-BN also has a hexagonal lattice, similar to graphene, with lattice mismatch of only 1.7% [21], the same behavior of graphene-OPA system should be expected for the h-BN-OPA case. Therefore, *ab initio* calculations were performed to investigate the relative stability of OPA self-assembled monolayers (SAMs)

atop h-BN, assuming that the OPA alkyl chains are oriented along either the armchair or the zigzag directions. The calculations were based on the density functional theory [22] within the local density approximation for the exchange-correlation functional, as implemented in the SIESTA method [23]. The same computational methodology as the one used in the previous study of OPA molecules atop graphene was adopted [20]. Concomitantly, h-BN flakes were decorated with OPA SAMs and investigated via AFM imaging [20].

Figure 2 sums up the results of both theoretical calculations and experiments. Figures 2a and 2b show the optimized geometries (top and side views) for the most stable OPA SAM configuration on h-BN. The calculations indicate that OPA alkyl chains oriented along the zigzag direction of h-BN is the most stable configuration, with the formation energy per OPA dimer 2.76 eV smaller than that along the armchair direction. As a consequence, the ripples formed by OPA headgroups should be oriented along the armchair direction (see Figure 2a). Figure 2c shows an AFM-phase image of an annealed few-layer h-BN flake completely covered by an OPA monolayer. A characteristic threefold wrinkle junction is evident in this image (in red colors), along with minor wrinkles on the top left. This image also shows ripples (in black colors) formed by the well-ordered phosphonic acid dimers. The FFT image (inset – bottom left) clearly identifies the periodicity of these ripples at 5nm, as expected by the *ab initio* results. These ripples are parallel to the wrinkle at the bottom right of figure 2c and form a 60 °angle with the other two wrinkles. Since ripples should be oriented along the armchair direction of h-BN, this indicates that wrinkles should also be oriented along the same direction. A careful inspection of the top left of figure 2c may indicate some ripple domains at an apparently different orientation. However, these ripples form a 120 °angle with the dominant ripple domain in the figure and, therefore, due to the C_3 symmetry of the system, are at the same armchair orientation. In summary, the OPA self-assembly investigation (both

theoretical and experimental) clearly indicates that the wrinkles formed on annealed h-BN are crystallographically oriented along its armchair direction.

2.3. Second Harmonic Generation experiments

In order to further verify the above statement, the wrinkle crystallographic orientation was studied by polarization dependent second harmonic generation (SHG) microscopy. For h-BN, the odd-layer samples belong to the D_{3h} point group symmetry, and the second order susceptibility tensor has a single non zero element [24, 25]. Thus, the dependence of the generated second harmonic intensity as a function of the sample angle for a pump laser polarization ($\hat{e}_{\omega}$) parallel to the analyzer ($\hat{e}_{2\omega}$) is

$$I(2\omega) = I \cos^2(3\Phi+\Phi_0) \qquad (1)$$

where Φ is the angle of the input laser polarization and the armchair direction and Φ_0 is the initial crystallographic orientation of h-BN sample.

Figure 3a and 3b show, respectively, the AFM and SHG images of an annealed h-BN flake with several wrinkles. In figure 3b, brighter colors mean stronger SHG intensity. A quick comparison between figure 3a and 3b indicate that the SHG signal is stronger at the wrinkles than at the flat regions of the flake. The intensity is proportional to the wrinkle height due to the increase in stress. We have measured SHG images rotating the sample (see sketch in the inset of figure 3b) and figure 3c shows the polar plot of the SHG intensity along the wrinkles as a function of the sample rotation angle Φ. The dots are the measured data and the red line is a fit of the data to equation 1 with $\Phi_0 = 0$, which clearly shows that the wrinkles are along the armchair direction. The intensity polar plot was measured for all the wrinkles in

figure 3b and they all show the same dependence. Additionally, the intensity polar plot on the area at the side of each wrinkle also shows the same dependence showing that they are oriented domains at an angle of 60 °with each other. In this sample, two wrinkles are not at the armchair direction (see grey arrows in figure 3a). Thus, as expected, they do not appear in the SHG image (figure 3b). Another interesting result from SHG measurements is that the h-BN flake sits flat on top of the Si substrate with well-oriented wrinkles, but without any compressive or tensile stress on the flat part of the flake. The strain occurs only at the wrinkles and their immediate vicinity.

3. Discussion

3.1. Phenomenological origami-like model and molecular dynamics simulations

It is known that h-BN has an atomically flat surface and, for this reason, it has been used as a substrate for graphene-based devices, since it increases carrier mobility by suppressing graphene undulations [21]. So, why this crystallographic wrinkling should occur? A possible reason lies in the annealing treatment and the difference between the thermal expansion coefficients of h-BN and the silicon substrate, in a similar mechanism to graphene wrinkling on CVD-grown and mechanically exfoliated flakes [6-10, 14]. However, there is a subtle difference in the h-BN/Si case: while Si behaves as a standard material and has a positive thermal expansion coefficient [1], h-BN has an anisotropic behavior: in the c-axis, the linear thermal expansion coefficient is positive and, thus, it behaves as a standard material in this axis. Yet, in the plane, the thermal expansion coefficient is negative [26]. Consequently,

h-BN layers shrink upon heating, while Si expands. On the other hand, during the cooling phase, h-BN expands while the substrate shrinks. Therefore, since the substrate anchors the flakes, it causes a tensile stress upon heating, flattening the flakes, and it causes a compressive stress upon cooling, crumpling them. In other words, the observed wrinkles should be a direct result of a two-dimensional compressive stress applied on the h-BN flakes by the Si substrate during the cooling phase of the annealing treatment. Basically, it is the same physical mechanism proposed for graphene wrinkling with two distinctions: the difference between graphene/substrate thermal expansion coefficients and the absence, so far, of reported observation of crystallographically-oriented wrinkles in graphene [6-10, 14]. One straightforward verification of such hypothesis is a direct comparison between the sum of wrinkle heights and the expected thermal expansion difference between the Si substrate and the h-BN flake: consider, for example, the h-BN flake of figure 1a, which is roughly 50 μm-long in any direction ($L \approx 50\mu m$). Any arbitrary line profile in this flake will cross several wrinkles. Adding the height of each crossed wrinkle yields a "total wrinkle height" H_W. At the same time, during the annealing process, the thermal expansion difference E_{th} between the Si substrate and the h-BN flake is simply $E_{th} = L(\alpha_{Si} - \alpha_{BN})\Delta T$, where α_{Si} (α_{BN}) is the thermal coefficient of Si (h-BN) and ΔT is the temperature variation in the annealing process. In any arbitrary line profile, we observe the approximate relationship $E_{th} \geq 2H_W$, which is a good indication that wrinkles are indeed created via the thermal expansion difference mechanism proposed above.

In order to create such well-organized and crystallographically oriented pattern of wrinkles, one should expect that the cooling phase (or, stress application) should be as slow as possible, allowing the system to achieve its lowest energy configuration. Indeed, crystallographic wrinkles are only observed when the annealing treatment is formed by a rapid heating step followed by a slow cooling phase. For example, good heating and cooling

rates for production of crystallographic wrinkles are 50 ℃ and 8 ℃, respectively. If faster cooling ramps are employed, only conventional, non-crystallographic and randomly oriented wrinkles are produced (Figure S1 – Supplementary material). A detailed investigation of what might the optimum heating and cooling rates for crystallographic wrinkle production be, also including other 2D materials [27], is out of the scope of the present work and is left as a natural step forward in this ongoing investigation.

If a uniform 2D compressive stress on a h-BN sheet may induce the formation of crystallographic wrinkles, then it is possible that it might be described by an origami-type folding pattern. In such a way, figure 4 shows a viable model for the origami-type formation of precisely-oriented wrinkle junctions. Figure 4a shows a schematic drawing of a feasible origami folding pattern. The black lines in figure 4a indicate regions where a fold may occur and their intersections form small triangles which are the unit cell of such origami pattern. The shaded regions in figure 4a indicate three wrinkles (and their junction) which are spontaneously formed when a 2D compressive stress is slowly applied to the sheet. As indicated by figure 4b, 4c and 4d, the model in figure 4a applies to h-BN, predicting wrinkle height and origami in a variety of sizes (larger than ~0.8 nm). Figure 4e illustrates the smallest possible wrinkle origami, which is formed by the small triangular unit cell in figure 4b. In other words, the model in figure 4 predicts crystallographically-oriented size-scalable wrinkles with triangular-shaped origami junctions. The striking similarities between the model in figure 4 and the AFM image in figure 1c, including the C_3 symmetry of the junction, give strong support to the assumption that the observed wrinkles are indeed the result of an origami-type folding of the h-BN sheet under a 2D compressive stress.

Even though the vast majority of wrinkles occurs in the armchair direction, it is possible to find a few wrinkles in the zigzag direction, as the topmost one pinpointed in figure

3a, and even some wrinkles that are oriented along neither armchair nor zigzag directions. The model of figure 4 can be modified so its triangular unit cell presents a zigzag edge. Also, in a continuum limit, figure 4a is consistent with wrinkles at any orientation. Then, what makes armchair-oriented wrinkles much more frequent than zigzag ones? In principle, the reason might lie either in the folding energetics or in fold dynamics, and it remains to be explained. Nevertheless, such armchair versus zigzag occurrence is a topic of interest in the research of any hexagonal 2D material. For example, it was recently observed that tearing monolayer graphene produces basically zigzag- and armchair-oriented edges, the latter being more common [28].

Finally, in order to verify the validity of the origami-like model of figure 4, molecular dynamics simulations were carried out for a biaxialy compressed h-BN layer atop an unstrained h-BN surface, within a periodic supercell approach. As an initial condition, shown in figure 5a, shallow ripples are imposed, forming a honeycomb superlattice akin to the wrinkle structure of figure 1b. As time evolves in the simulation (see video in supporting information), the wrinkle structure increases in height and modifies its shape, as the compressive strain of the planar part of the BN layer is relaxed. The final, stable wrinkle structure (after 120 ps) is shown in figure 5b. The final junction structure shows the characteristic rotated-triangle shape seen in both the experimental morphology (figure 1c) and the origami model of figure 4.

It is important to note the spontaneous symmetry breaking which occurred during the molecular dynamics simulation, and that such symmetry breaking is consistent with the experiments. The symmetry of the initial ripple junction, shown in figure 5a, is C_{3v}, with mirror symmetry across the cell large diagonal (which is along the armchair direction). The symmetry of the final wrinkle junction, shown in figure 5b, is C_3, without such mirror

symmetry. The latter is, in fact, the symmetry of the experimental wrinkle junctions. Therefore, the mechanical characteristics of h-BN allows for the spontaneous formation of origami-type structures in response to biaxial compression.

4. Conclusion

In conclusion, this work reports on origami-type wrinkles created on h-BN through a straightforward strain engineering procedure: thermally-induced progressive 2D compressive stress application. In other words, origami-type folding and wrinkling might be a general property of any 2D material, if proper strain engineering conditions are provided. Hexagonal-lattice 2D materials, like h-BN and graphene should present the same origami pattern [27], whereas different surface lattices, like those of 2D chalcogenides (encompassing metals, semiconductors and topological insulators: MoS_2, WS_2, $MoTe_2$, Bi_2Se_3 and others) could yield topologically different origami patterns. Such wrinkle engineering could be ultimately used for generating and controlling new "pseudomagnetic", flexoelectric and photonic effects on specific 2D materials.

5. Experimental Section

Sample preparation and AFM characterization: Hexagonal boron nitride flakes were prepared by standard mechanic exfoliation using commercial h-BN powder (Sigma-Aldrich) [29]. The exfoliated flakes were transferred onto a doped Si substrate with a thin layer (300 nm) of silicon oxide and annealed at 1000 ℃ for 25 minutes in a quartz tube. Heating and cooling rates for

crystallographic wrinkles production were 50 ℃/min and 8 ℃/min, respectively. Atomic force microscopy characterization of the samples was carried out on Bruker MultiMode 8 and on Park XE-70 microscopes operating in PeakForce and intermittent contact modes, respectively. Silicon cantilevers (from Bruker, Mikromasch and Nanosensors), with spring constants ranging from 0.5 to 40 N/m and tip radius of curvature around 10nm, were employed throughout the work for sample imaging.

Second Harmonic Generation experiments: The SHG microscopy system uses a 140 fs Ti-Sapphire laser which is directed to a confocal scanning laser microscope modified for two photon excitation. The laser (wavelength 800 nm) is focused on the sample at normal incidence by a 40X objective. The SH back reflected signal at 400 nm is collected by the same objective and directed by a dichroic mirror to a thin bandpass filter (20 nm) centered at the SH wavelength and a polarizer analyzer to be detected by a photomultiplier tube. The sample is mounted on a rotation stage for the polarization dependence measurements.

Molecular Dynamics simulations: Molecular dynamics (MD) technique, as implemented in LAMMPS package [30], was used to simulate a h-BN bilayer in the canonical ensemble. The bottom layer, representing the unstrained h-BN surface, consists of a 40x40 periodic supercell of 3200 atoms. Those atoms were not subject to strain and the resultant forces on them were set zero in all simulations. The strained h-BN upper layer was represented by a 44x44 supercell of 3872 atoms biaxially compressed by 1/11 such that its lattice vectors coincide with those of the unstrained h-BN surface. In the initial condition, shown in Figure 5a, shallow ripples are imposed by increasing the z coordinates of the B and N atoms in a gaussian profile, forming a honeycomb superlattice akin to the wrinkle structure of Figure 1b. For the interactions between atoms, we have used the Tersoff potential [31] with parameters given by Albe and Möller [32]. Additionally to the Tersoff potential, a force field acting on each atom, perpendicular to and directed towards the h-BN surface, was considered to represent van der Waals interactions

between planes. Such force field is given by $F=4a.d^{-5}$ [33], where d is the distance from the plane that contains the atoms of the bottom layer, and a = 4.3 eVÅ^4. The temperature was kept constant at 10 K through Nosé-Hoover thermostat [34, 35]. The time step was 0.0002 ps and the total simulation time was 120 ps (or 6 million MD steps).

Supplementary material

Supplementary material shows AFM images of h-BN flakes submitted to fast cooling treatments showing conventional, non-organized wrinkles. Video showing the time evolution of h-BN wrinkles in molecular dynamics simulations. Supplementary material is available in the online version of this article at http://dx.doi.org/10.1007/**********)

Acknowledgments

The authors are thankful to Prof. Rodrigo Gribel for the use of the laboratory facilities. All authors acknowledge financial support from Coordenação de Aperfeiçoamento de Pessoal de Nível Superior (Capes), Conselho Nacional de Desenvolvimento Científico e Tecnológico (CNPq), Fundação de Amparo à Pesquisa do estado de Minas Gerais (Fapemig), Rede Nacional de Pesquisa em Nanotubos de Carbono and Instituto Nacional de Ciência e Tecnologia (INCT-Nano-Carbono).

References

[1] Bower, A. F. *Applied Mechanics of Solids*; CRC Press: Florida, 2009.

[2] Lakes, R. Foam structures with a negative Poisson's ratio. *Science* **1987,** *235*, 1038-1040

[3] Baughman, R. H.; Stafstrom, S.; Cui, C.; Dantas, S. O. Materials with Negative Compressibilities in One or More Dimensions. *Science* **1998**, *279*, 1522−1524.

[4] Barboza, A. P. M.; Chacham, H.; Oliveira, C. K.; Fernandes, T. F. D.; Martins Ferreira, E. H.; Archanjo, B. S.; Batista, R. J. C.; de Oliveira, A. B.; Neves, B. R. A. Dynamic Negative Compressibility of Few-Layer Graphene, h-BN, and MoS_2. *Nano Lett.* **2012**, *12*, 2313-2317.

[5] Cairns, A. B.; Catafesta, J.; Levelut, C.; Rouquette, J.; van der Lee, A.; Peters, L.; Thompson, A. L.; Dmitriev, V.; Haines, J.; Goodwin, A. L. Giant negative linear compressibility in zinc dicyanoaurate. *Nat. Materials* **2013**, *12*, 212-216.

[6] Obraztsov, A.N.; Obraztsova, E.A.; Tyurnina A.V.; Zolotukhin, A.A. Chemical vapor deposition of thin graphite films of nanometer thickness. *Carbon* **2007**, *45*, 2017-2021.

[7] Li, X.; Cai, W.; An, J.; Kim, S.; Nah, J.;Yang, D.; Piner, R.; Velamakanni, A.; Jung, I.; Tutuc, E.; Banerjee, S. K.; Colombo, L.; Ruoff, R. S.Large-area synthesis of high-quality and uniform graphene films on copper foils. *Science* **2009**, *324*, 1312–1314.

[8] Xu, K.; Cao, P.; Heath, J.R. Scanning tunneling microscopy characterization of the electrical properties of wrinkles in exfoliated graphene monolayers. *Nano Lett.* **2009,** *9*, 4446–4451.

[9] Robertson, A.W.; Bachmatiuk, A.; Wu, Y. A.; Schäffel, F.; Büchner, B.; Rümmeli, M. H.; Warner, J. H.; Structural distortions in few-layer graphene creases. *ACS Nano* **2011,** *5*, 9984–9991.

[10] Zhu, W.; Low, T.; Perebeinos, V.; Bol, A. A.; Zhu, Y.; Yan, H.; Tersoff, J.; Avouris, P. Structure and electronic transport in graphene wrinkles. *Nano Lett.* **2012,** *12*, 3431–3436.

[11] Huang, Y.; Wu, J.; Xu, X.; Ho, Y.; Ni, G.; Zou1, Q.; Kok, G.; Koon, W.; Zhao, W.; Castro Neto, A. H.; Eda, G; Shen, C; Özyilmaz, B. An innovative way of etching MoS_2: Characterization and mechanistic investigation. *Nano Research* **2013**, *6*, 200–207.

[12] Lherbier, A.; Roche, S.; Restrepo, O. A.; Niquet, Y.-M.; Delcorte, A.; Charlier, J.-C.; Highly defective graphene: A key prototype of two dimensional Anderson insulators. *Nano Research* **2013**, *6*, 326–334.

[13] Shaw, J. C.; Zhou, H.; Chen, Y.; Weiss, N. O.; Liu, Y.; Huang, Y; Duan, X.; Chemical vapor deposition growth of monolayer $MoSe_2$ nanosheets. *Nano Research* **2014**, *7*, 511–517.

[14] Zhang, K.; Arroyo, M.; Understanding and strain-engineering wrinkle networks in supported graphene through simulations. *J. Mech. Phys. Solids* **2014**, *72*, 61–74.

[15] Guinea, F.; Katsnelson, M. I.; Geim, A. K. Energy gaps and a zero-field quantum hall effect in graphene by strain engineering. *Nat. Phys.* **2010**, *6*, 30–33.

[16] Feng, J.; Qian, X.; Huang, C.-W.; Li, J. Strain-Engineered Artificial Atom as a Broad-Spectrum Solar Energy Funnel. *Nat. Photonics* **2012**, *6*, 866-872.

[17] Naumov, I.; Bratkovsky, A. M.; Ranjan, V. Unusual flexoelectric effect in twodimensional noncentrosymmetric sp^2-bonded crystals. *Phys. Rev. Lett.* **2009**, *102*, 217601.

[18] Roy, K.; Bandyopadhyay, S.; Atulasimha, J. Hybrid spintronics and straintronics: A magnetic technology for ultra-low energy computing and signal processing. *Appl. Phys. Lett* **2011**, *99*, 063108.

[19] Pan, Z.; Liu, N.; Fu, L.; Liu, Z. Wrinkle Engineering: A New Approach to Massive Graphene Nanoribbon Arrays. *J. Am. Chem. Soc.* **2011**, *133*, 17578–17581.

[20] Prado, M. C.; Nascimento, R.; Moura, L. G.; Matos, M. J. S.; Mazzoni, M. S. C.; Cancado, L. G.; Chacham, H.; Neves, B. R. A. Two-dimensional molecular crystals of phosphonic acids on graphene. *ACS Nano* **2011**, *5*, 394–398.

[21] Dean, C. R.; Young, A. F.; Meric, I.; Lee, C.; Wang, L.; Sorgenfrei, S.; Watanabe, K.; Taniguchi, T.; Kim, P.; Shepard, K. L.; Hone, J. Boron nitride substrates for high-quality graphene electronics. *Nature Nanotechnology* **2010**, *5*, 722-726.

[22] Kohn, W.; Sham, L. J. Self-Consistent Equations Including Exchange and Correlation Effects. *Phys. Rev.* **1965**, *40*, A1133-A1138.

[23] Soler, J. M.; Artacho, E.; Gale, J. D.; Garcia, A.; Junquera, J.; Ordejon, P.; Sanchez-Portal, D. The SIESTA Method for Ab Initio Order-N Materials Simulation. *Condens. Matter* **2002**, *14*, 2745–2779.

[24] Malard, L. M.; Alencar, T. V.; Barboza, A. P. M.; Mak, K. F.; de Paula, A. M. Observation of intense second harmonic generation from MoS_2 atomic crystals. *Phys. Rev. B* **2013**, *87*, 201401.

[25] Y Li, Y.; Rao, Y.; Mak, K. F.; You, Y.; Wang, S.; Dean, C. R.; Heinz, T. F. Probing symmetry properties of few-layer MoS_2 and h-BN by optical second-harmonic generation. *Nano Lett.* **2013**, *13*, 3329–3333.

[26] Paszkowicz, W.; Pelka, J.B.; Knapp, M.; Szyszko, T.; Podsiadlo, S. Lattice parameters and anisotropic thermal expansion of hexagonal boron nitride in the 10–297.5 K temperature range. *Appl. Phys. A* **2002**, *75*, 431–435.

[27] An attempt to reproduce on graphene the observed origami-wrinkles on h-BN was made following exactly the same experimental procedure. However, all graphene flakes burnt out during the annealing cycle, as graphene is not as thermal resistant as h-BN. See: Li, L. H.;

Cervenka, J.; Watanabe, K.; Taniguchi, T.; Chen, Y. Strong Oxidation Resistance of Atomically Thin Boron Nitride Nanosheets. *ACS Nano* **2014**, *8*, 1457-1462.

[28] Kim, K.; Artyukhov, V. I.; Regan, W.; Liu, Y.; Crommie, M. F.; Yakobson, B. I.; Zettl, A. Ripping Graphene: Preferred Directions. *Nano Lett.* **2012**, *12*, 293-297.

[29] Oliveira, C. K.; Matos, M. J. S.; Mazzoni, M. S. C.; Chacham, H.; Neves, B. R. A. Anomalous response of supported few-layer hexagonal boron nitride to DC electric fields: a confined water effect? *Nanotechnology* **2012**, *23*, 175703.

[30] Plimpton, S. J. Fast Parallel Algorithms for Short-Range Molecular Dynamics. *J. Comp. Phys.* **1995**, *117*, 1-19.

[31] Tersoff, J. New empirical approach for the structure and energy of covalent systems. *Phys. Rev. B* **1988**, *37*, 6991.

[32] Albe, K.; Möller, W. Modelling of boron nitride: Atomic scale simulations on thin film growth. *Comp. Mat. Sci.* **1998**, *10*, 111-115.

[33] Dappe, Y. J.; Basanta, M. A.; Flores, F.; Ortega, J. Weak chemical interaction and van der Waals forces between graphene layers: A combined density functional and intermolecular perturbation theory approach. *Phys. Rev. B* **2006**, *74*, 205434.

[34] Nosé, S. A unified formulation of the constant temperature molecular dynamics methods. *J. Chem. Phys.* **1984**, *81*, 511.

[35] Hoover, W. G. Canonical Dynamics: Equilibrium phase-space equations. *Phys. Rev. A* **1985**, *31*, 1695.

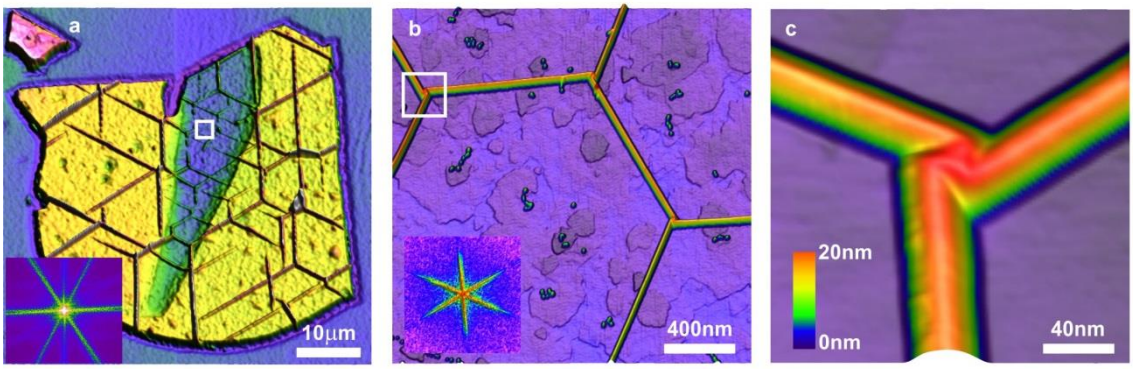

Figure 1. AFM characterization of h-BN flakes after annealing. (a) A 10nm-thick flake showing an orientationally ordered wrinkle pattern. The inset at the bottom left shows the FFT image of the flake topography. (b) Zoom-in AFM image acquired at the region marked by a white square in (a). The wrinkle pattern orientation is evidenced by the FFT image at the bottom left of the figure. (c) Detailed topographic image of the wrinkle junction indicated by the white square in b. The color scale at the bottom left of the image indicates its height variation.

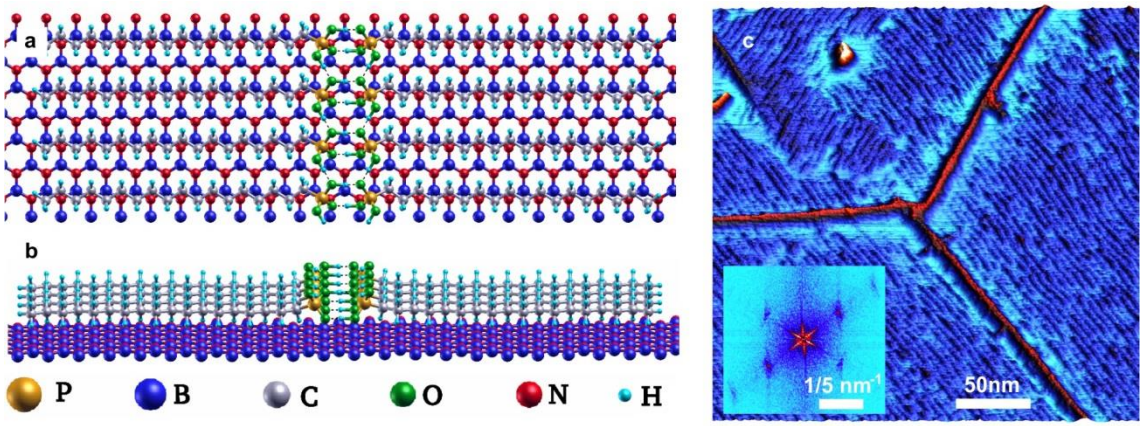

Figure 2. Theoretical and experimental investigation of OPA self-assembly on h-BN. (a, b) Detailed views (top view – a, side view – b) of the most stable OPA structure atop h-BN obtained the in calculations. (c) AFM-Phase image of an annealed h-BN flake decorated with

OPA SAMs which form parallel ripples across the sample surface (Flake thickness: 8nm). The inset shows the FFT image of the same region, evidencing the periodicity and orientation of the ripples.

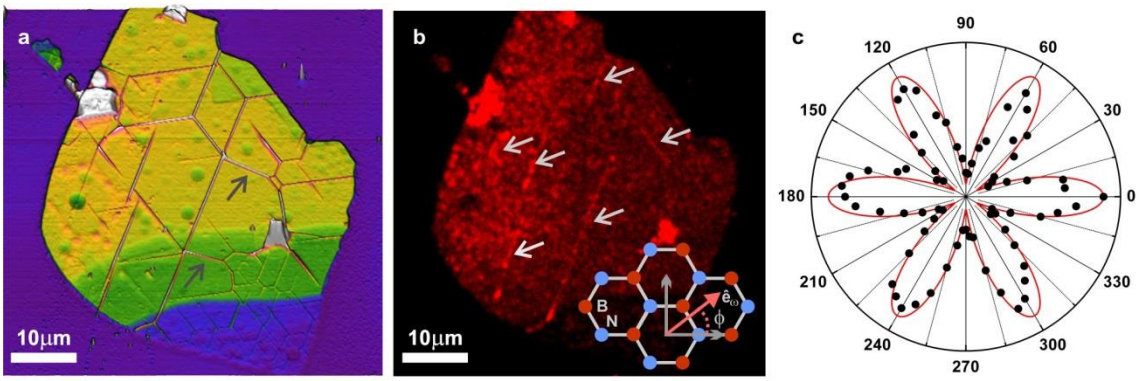

Figure 3. Second Harmonic Generation characterization of wrinkles. (a) AFM image of a 28nm-thick h-BN flake after annealing showing several wrinkles. The grey arrows indicate two wrinkles in non-armchair orientations. (b) SHG image of the same h-BN flake. In the image, brighter colors indicate stronger SHG intensity. Several wrinkles, which yield large SHG signals, are indicated by arrows. The inset on the bottom right shows a sketch of the h-BN structure, indicating the angle between the laser polarization and the armchair direction x. (c) Polar plot of the SHG intensity along the wrinkles as a function of the sample rotation angle.

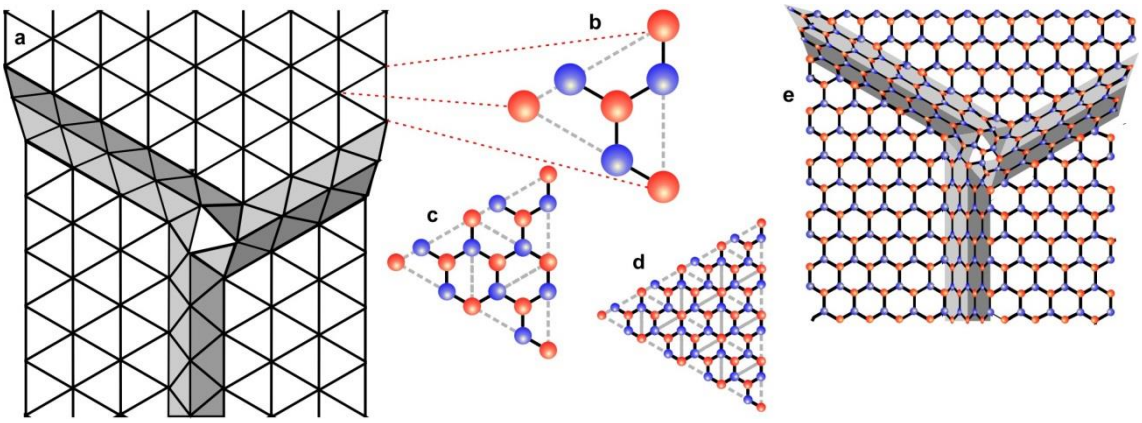

Figure 4. The origami-like model for the wrinkle junctions. (a) Schematic drawing of the proposed origami-like folding of a h-BN sheet. The unit cell in this model is a triangle, which can be scaled to a variety of sizes, as indicated by figures (b), (c) and (d). (e) Proposed model for the smallest possible h-BN wrinkle junction: the wrinkles are along the armchair direction and their junction forms a small triangle at the center.

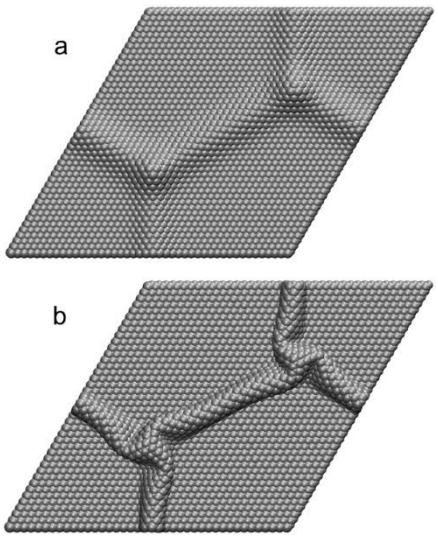

Figure 5. Molecular dynamics simulations of wrinkle junction formation. (a) Initial top layer configuration used for MD simulations of a biaxially compressed BN layer atop a fixed, unstrained, one (not shown). (b) Final, stable wrinkle structure obtained after 120 ps (or 6 million MD steps). Note the spontaneous symmetry breaking from the initial to the final states of the wrinkle junction, from C_{3v} to C_3, respectively and its rotated triangular morphology.

Supplementary material

Crystal-oriented wrinkles with origami-type junctions in few-layer h-BN

Camilla K. Oliveira, Egleidson F. A. Gomes, Mariana C. Prado, Thonimar V. Alencar, Regiane Nascimento, Leandro M. Malard, Helio Chacham, Ana M. de Paula and Bernardo R. A. Neves[*]

1. Sample Quenching

Boron Nitride samples were heated at a rate of 8 ℃ and were then quickly removed from the furnace. If faster cooling ramps are employed, only conventional, non-crystallographic and randomly oriented wrinkles are produced.

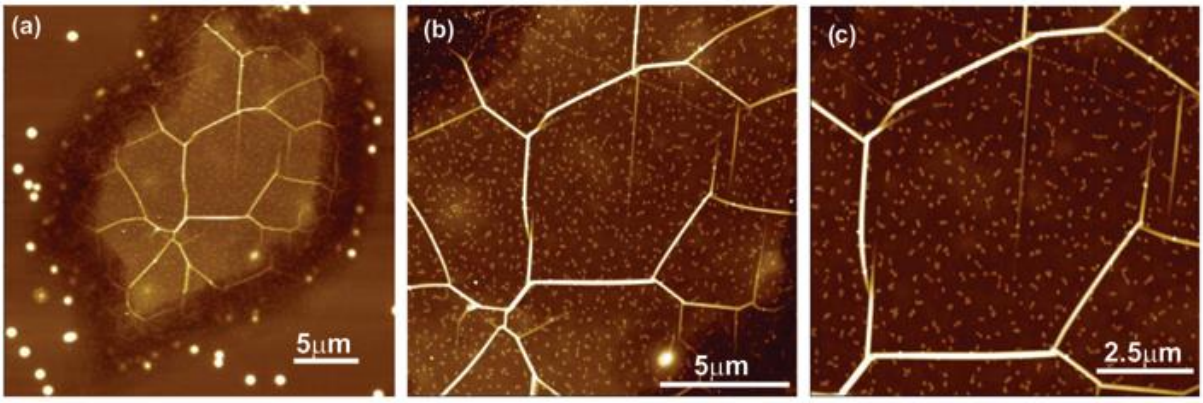

Figure S1. AFM characterization of few-layer h-BN flakes after slow annealing and quenching. a) A flake showing a non-orientationally ordered wrinkle pattern. (b) Zoom-in AFM image from image (a). (c) Zoom-in AFM image from image (b).